European Journal of Pharmaceutics and Biopharmaceutics 74 (2010) 41–49

Contents lists available at ScienceDirect

European Journal of Pharmaceutics and Biopharmaceutics

journal homepage: www.elsevier.com/locate/ejpb

Research paper

Micro-CT in drug delivery

Yiwei Wang [a], David F. Wertheim [b], Allan S. Jones [c], Allan G.A. Coombes [a,*]

[a] The University of Queensland, School of Pharmacy, Brisbane, Qld, Australia
[b] Faculty of Computing, Information Systems and Mathematics, Kingston University, Kingston upon Thames, Surrey, UK
[c] Australian Key Centre for Microscopy and Microanalysis, University of Sydney, NSW, Australia

ARTICLE INFO

Article history:
Received 12 January 2009
Accepted in revised form 14 May 2009
Available online 22 May 2009

Keywords:
Micro-CT
Drug delivery
Matrix

ABSTRACT

Micro-computed tomography (micro-CT) has not to date been fully exploited in the area of controlled drug delivery despite its capability for providing detailed, 3-D images of morphology and the opportunity this presents for exploring the relationships between delivery device formulation, structure and performance. Micro-CT was used to characterize the internal structure of polycaprolactone (PCL) matrix-type devices incorporating soluble particulates (lactose Mw 342.30, gelatin Mw 20–25 kDa) as models of hydrophilic bioactives or pore-forming excipients. Micro-CT images confirmed that the lactose and gelatin particles were uniformly dispersed throughout the PCL phase and that efficient delivery of 95–100% of each species in 9 days involved transport from the matrix core. Quantitative analysis of micro-CT images provided values for matrix macroporosity, which were within 15% of the theoretical value and revealed uniform porosity throughout the samples. Total release of protein occurred in 9 days (PBS, 37 °C) from matrices containing a high protein load (44% w/w) and was independent of particle size. Measurements of equivalent pore diameter and frequency distribution identified a large population of sub-40 μm pores in each material, indicative of a high density of connecting channels between particles which facilitates protein transport through the matrices.

1. Introduction

Controlled drug release devices are designed to release bioactives at a defined rate, over a set time period to achieve therapeutic effects at local or systemic level. Implantable, topical and insertable devices are often based on matrix-type designs in which drug particulates are distributed throughout a polymeric phase (Fig. 1). Such devices have been widely investigated for use in hormone replacement therapy, contraception, ocular drug delivery, treatment of cancer, control of bacterial infection [1–5] and more recently for production of tissue engineering scaffolds which incorporate growth factors [6]. The overall rate and pattern of drug release from matrix systems are determined by various factors including the physico-chemical properties of the drug and polymer, the pore structure of the matrix (pore size, percentage porosity, connectivity and tortuosity) (Fig. 1), drug diffusion through fluid-filled pores and channels (and/or the polymer itself), polymer dissolution, erosion or degradation. The kinetics of drug release from matrix-type devices incorporating dispersed drug in particulate form (where release occurs through fluid-filled pores in the matrix) are frequently controlled by Fickian diffusion and conveniently described by the Higuchi equation [7].

$$Q = \sqrt{tCsD\frac{\varepsilon}{\tau}(2C - \varepsilon Cs)}$$

where Q is the amount of drug released in time t, C is the initial drug concentration, Cs is the drug solubility in the release medium, D is the diffusion coefficient of drug molecules in the release medium, τ is the tortuosity, ε is the matrix porosity.

Various techniques have been applied to characterize the porosity of materials including theoretical approaches, scanning electron microscopy (SEM), mercury porosimetry, gas pycnometry and adsorption. However, there are significant practical issues associated with these measurements. Techniques such as mercury porosimetry and gas flow porometry can be used to estimate pore size distributions but these typically differ by an order of magnitude due to differences in the underlying physics of the techniques [8]. Electron and other microscopies are extensively used to produce images of porous materials but the challenge is again to quantify the dimensions of structural features such as pores and connecting channels having irregular shapes and sizes. Furthermore, neither mercury porosimetry nor gas adsorption methods can account for closed pores, whilst mercury porosimetry only measures the distribution of constrictions in a pore network.

Pore tortuosity (defined as the ratio of the actual path length through connected pores to the Euclidean distance (shortest linear distance) plays a key role in controlling drug delivery from matrix-type devices but is rarely quoted in the literature. Calculation of

* Corresponding author. The University of Queensland, School of Pharmacy, St. Lucia, Brisbane, Qld 4072, Australia. Tel.: +61 7 33451372; fax: +61 7 33651688.
E-mail address: a.coombes@pharmacy.uq.edu.au (A.G.A. Coombes).

0939-6411/$ - see front matter © 2009 Elsevier B.V. All rights reserved.
doi:10.1016/j.ejpb.2009.05.008

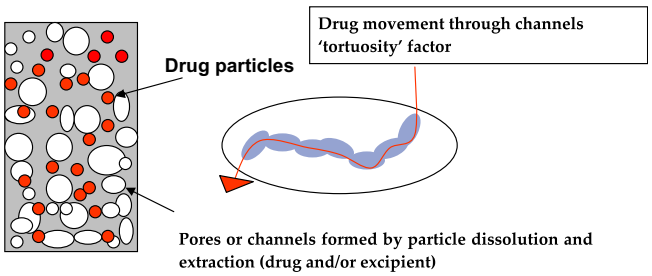

Fig. 1. Schematic of drug delivery from porous matrice.

tortuosity values using measurements of drug dissolution from a matrix [9,10] can result in unrealistic numerical values of more than 1000 [11] or below one [9]. Tortuosity has been measured using porosity and diffusion coefficients obtained from spin echo NMR measurements [12]. Mercury intrusion porosimetry has also been suggested for determining tortuosity. Wu et al. [12] recently described a method to find the shortest route through the pores in images of compacts using an algorithm called 'grey-weighted distance transform (GDT)' which provide precise measurements of tortuosity.

The pore structure of the matrix may be produced during formulation or generated by solubilisation of drug and excipient (Fig. 1) but regardless of the mechanism of pore formation, detailed quantitative analysis of the pore architecture to define porosity and turtuosity parameters would be anticipated to lead to improvements in device design, quality control and drug release behaviour. Micro-computed tomography (micro-CT) provides detailed 3-D images of the internal structure of materials by combining X-ray transmission techniques with computed tomographical reconstruction (Fig. 2). A scanning X-ray beam transmitted through the specimen generates a set or sequence of 2-D shadow images (absorption images or grey-scale images) due to density differences within the specimen that affects the intensity of transmitted radiation. Internal features of the material can be visualised in 3-D from the 2-D images and further analysed to provide two- and three-dimensional morphological parameters such as pore shape, size, connectivity and pore distribution [13,14]. Feldkamp et al. [15] pioneered micro-CT imaging technology to analyze trabecular bone samples at a spatial resolution of 50 μm. Since then, micro-CT has been used extensively in the study of bone architecture and other tissue types including vasculature and lung tissue. More recently, a number of investigators have recognized the advantages of the technique for characterizing the pore structure of implantable scaffolds which are designed to support and guide growth of new tissue. Micro-CT has also provided design parameters for modeling the mechanical performance of such materials. Williams et al. [16] recently used micro-CT to assess the porosity of polycaprolactone (PCL) scaffolds produced by selective laser sintering and subsequent bone formation following cell seeding and implantation in mice. Jones et al. [13] used micro-CT and image analysis to identify pores, interconnects and the pore size distribution in bioceramic scaffolds in order to optimize the permeability of the material for cell seeding. A decided advantage of micro-CT lies in acquisition of 3-D image datasets of the internal structure of materials at microscopic resolution, whereas SEM is limited to surface analysis of relatively small fields of view. Micro-CT is also potentially capable of discriminating between related structural features, for example isolated pores in a continuous polymer phase and interconnected pores linked by narrow throats (connects) in more complex formats [17]. However, the same argument about quantification of the dimensions of structural features in electron and other microscopies applies to micro-CT. For example, calculations based on analysis of a series of scaffold images obtained from a tomographical method depend on how well the boundaries of the voids or pores can be defined, on the instrument resolution in x and y or x, y and z planes and on the vertical distance between sequential images. Furthermore, micro-CT analysis is time consuming and the resolution of images is limited to 5–10 μm.

Micro-computed tomography [18] has not to date been fully exploited in the area of controlled drug delivery despite its potential for clarifying the relationships between delivery device formulation, structure and performance. Here we demonstrate the utility of micro-CT for characterizing the internal structure of matrix-type devices incorporating soluble particulates (lactose, Mw 342.3, gelatin, Mw 20–25 kDa) as models of hydrophilic bioactives and pore-

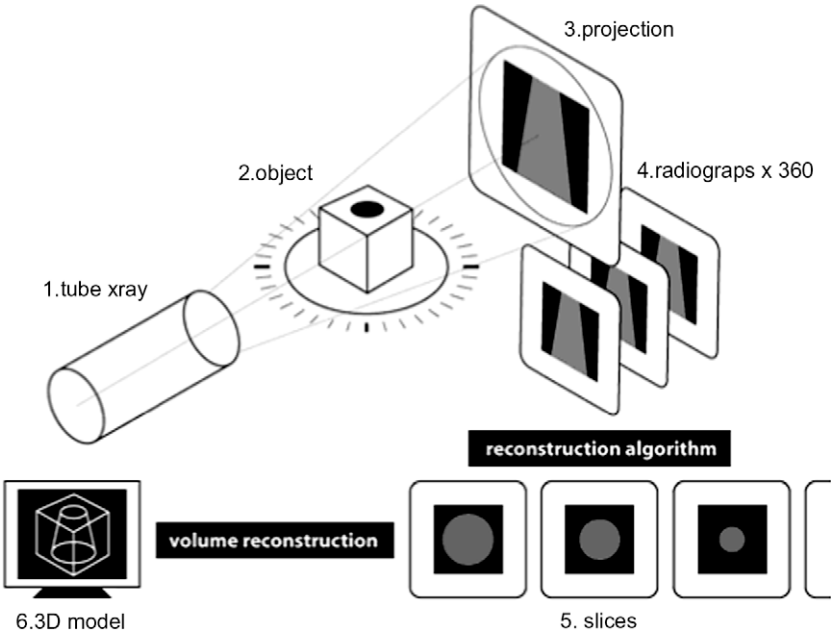

Fig. 2. The principle of computed micro-tomography (micro-CT).

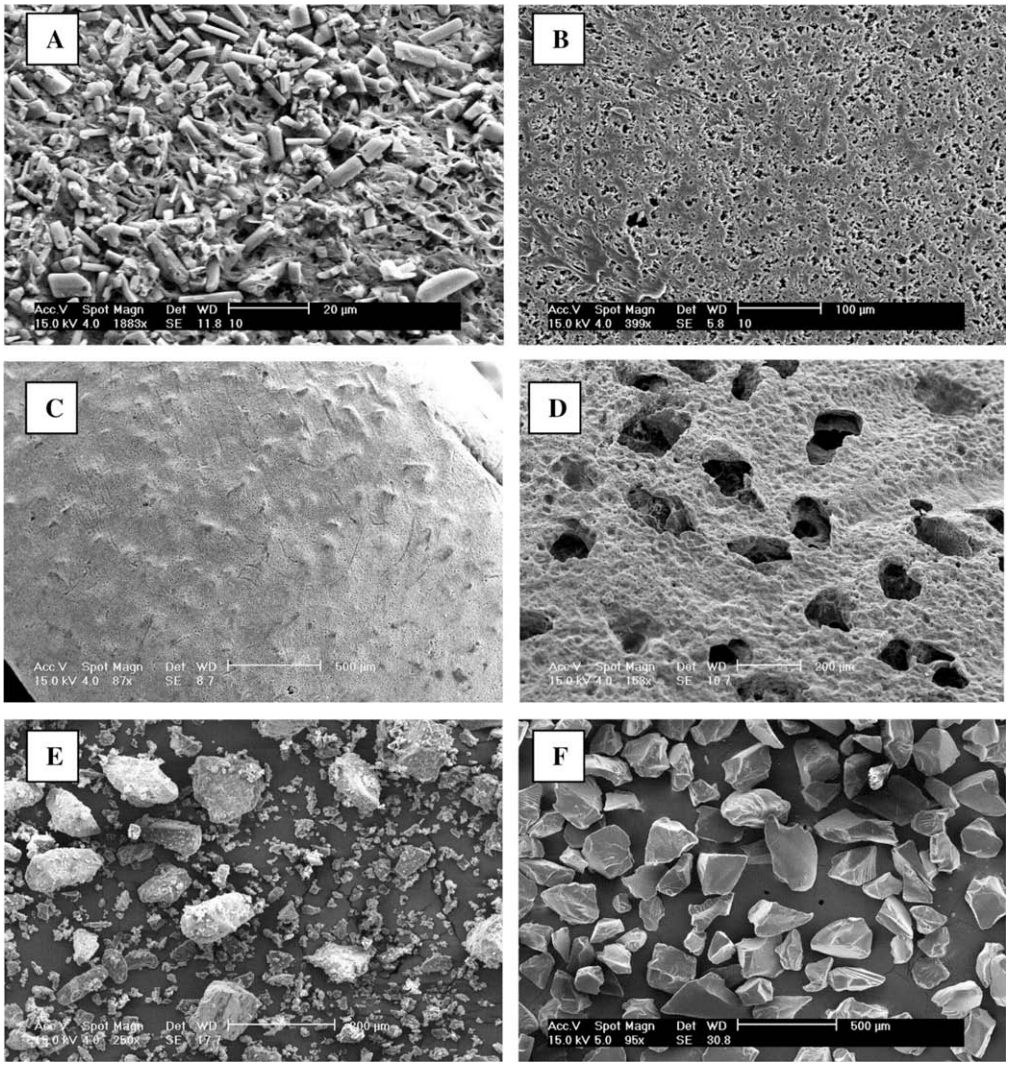

Fig. 3. Scanning electron micrographs of (A) lactose (125–250 µm): PCL matrix before release (B) lactose (125–250 µm): PCL matrix after release (C) gelatin (125–250 µm): PCL matrix before release (D) gelatin (125–250 µm): PCL matrix after release (E) lactose particles (F) gelatin particles.

forming excipients. Quantitative analysis of micro-CT images provided information on macroporosity, pore size and frequency distribution of pore size for correlation with release behaviour. The direct relationship between the macroporous structure formed by particle extraction and the original distribution of particulates in the matrix yielded a sensitive quality control measure for evaluating material uniformity and its relationship with formulation conditions.

2. Materials and methods

2.1. Production of PCL matrices incorporating lactose and gelatin particulates

Polycaprolactone (PCL) matrices incorporating lactose and gelatin particulates, respectively, were produced by a rapid cooling method. PCL (1.7 g, Mw 115 kDa, CAPA 650, Solvay Interox, Warrington, UK) was dissolved in 10 ml acetone by gentle heating at approximately 50 °C to produce a 17% w/v solution. Lactose particles in three size ranges (45–90, 90–125, 125–250 µm) were obtained by sieving the as-received powder (Sigma, Australia). Each defined size range (insoluble in acetone) was dispersed in the PCL solution using a glass rod to give a final concentration of 29% w/w. Gelatin powder (Type B, bloom 125 purchased from Sigma) insoluble in acetone, was sieved to obtain particle size ranges of 45–90, 90–125 and 125–250 µm and dispersed, respectively, in

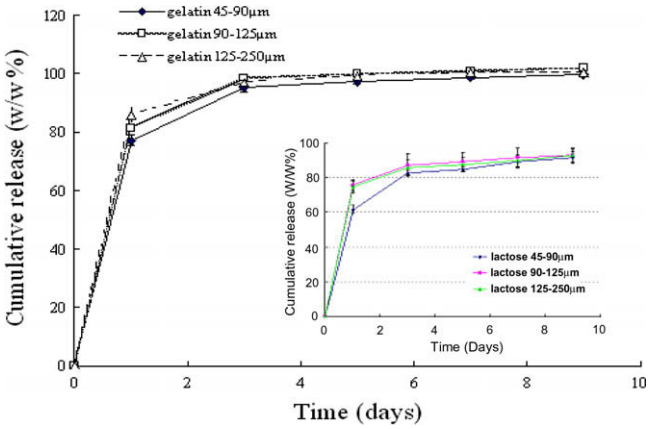

Fig. 4. Cumulative lactose release from microporous PCL matrices (29% w/w particle loading) and gelatin release from microporous PCL matrices (44% w/w particle loading) containing discrete particle size ranges.

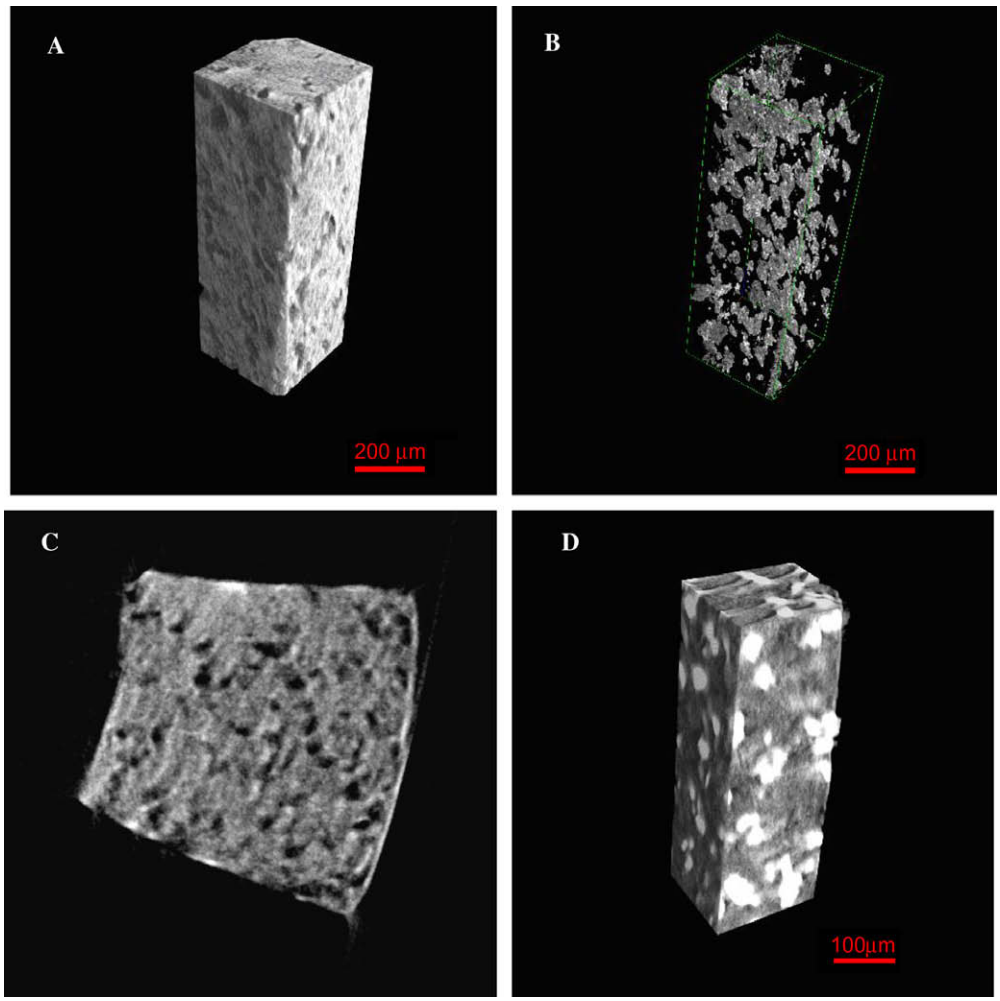

Fig. 5. Internal microtomographs of (A) Polymeric phase of 29% w/w lactose (125–250 μm): PCL matrix after release (B) Pore structure of 29% w/w lactose (90–125 μm): PCL matrix after release (C) 2-D shadow images of 29% w/w lactose (45–90 μm): PCL matrices after release (D) 29% w/w gelatin (125–250 μm): PCL matrix before release (light regions correspond to the gelatin particles) (E) Polymeric phase of 29% w/w gelatin (90–125 μm): PCL matrix after release (F) Pore structure of 29% w/w gelatin (125–250 μm): PCL matrix after release (G) Pore structure of 29% w/w gelatin (45–90 μm): PCL matrix after release (H) 2-D shadow images of 29% w/w gelatin (45–90 μm): PCL matrix after release.

PCL solution to produce three protein concentrations of 29, 38 and 44% w/w, respectively. The suspensions were transferred into a mould comprising a 3 ml polypropylene (PP) syringe body with a centrally located 1 ml PP syringe body. After cooling in dry ice (−78 °C) for 2–5 min to induce rapid crystallization and hardening of the polymer, the matrices were removed from the mould and immersed in methanol (50 ml) for 24 h to extract the acetone. The matrices were removed from the methanol bath and the acetone/methanol remaining in the matrices was allowed to evaporate in air under ambient conditions.

2.2. Lactose and gelatin release from PCL matrices

Samples of lactose-loaded PCL matrices (100 mg) were accurately weighed and immersed in 10 ml distilled water at 37 °C for 15 days. The release medium was replaced completely by fresh distilled water at 1-day intervals and the concentration of lactose in the samples was determined by HPLC (Waters). The amount of lactose release was calculated using a calibration curve and expressed as cumulative release (%) versus time. Accurately weighed samples of PCL matrices loaded with gelatin powder in various particle size ranges were immersed in 10 ml PBS (pH 7.4). The sample tubes were retained at 37 °C for 21 days and the release medium was replaced completely by fresh PBS at 1-day intervals. The amount of gelatin release was analysed after 24 h and then every 2 days up to 21 days using the BCA total protein assay and expressed as cumulative release (% w/w) versus time.

2.3. Scanning electron microscopy

The morphology of lactose or gelatin-loaded PCL matrices before and after release were examined using a Philips XL30 scanning electron microscope (SEM). Samples were mounted on aluminum sample stubs and sputter coated with platinum prior to examination in the SEM at a voltage of 15 kV

2.4. Micro-CT image acquisition

Longitudinal samples (approximately 2 × 2 × 10 mm in length) were cut from microporous PCL tubes and analysed using a Skyscan1072 (Skyscan, Aartselaar, Belgium) desktop X-ray CT scanner at 15 μm voxel resolution (50× magnification), X-ray tube current of 173 μA and voltage of 30 kV. Specimens were mounted vertically on a plastic support and rotated through 360° around the long axis (*z*-axis) of the sample. The absorption image was recorded every 0.225° of rotation. These projection radiographs were then

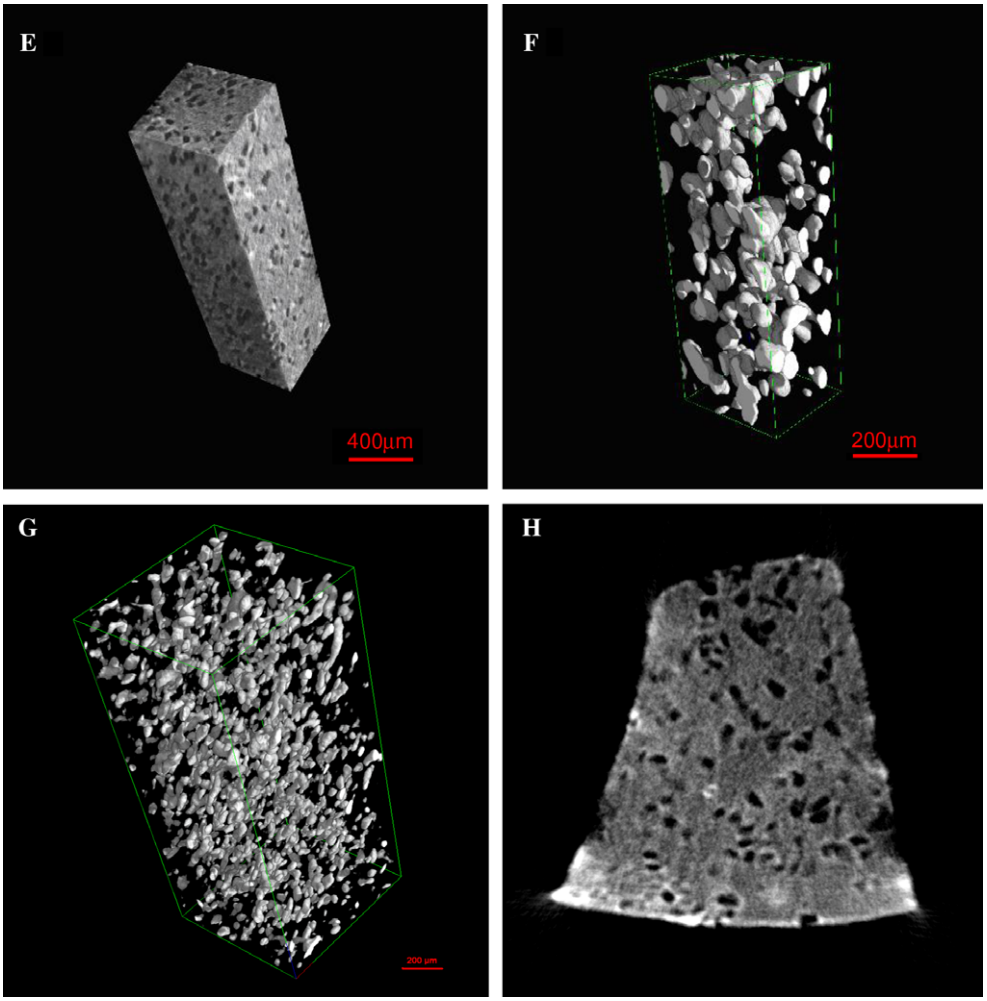

Fig. 5 (*continued*)

used in standard cone-beam reconstruction software to generate a series of 1024 8bit axial slices, each of 1024 × 1024 pixels, that had *Z*-dimensional spacing equal to the within slice pixel spacing. The resulting 3-D data sets were hence isotropic with voxel spacing of 15 µm over the entire 1024^3 spatial range. Three-dimensional reconstruction of the internal pore morphology was carried out using these axial bitmap images and analysed by VG Studio Max 1.2 software (Volume Graphics GmbH, Heidelberg, Germany).

2.5. Quantitative analysis of micro-CT images

Analysis of transverse micro-CT images obtained at 1000 µm intervals along the sample long-axis was performed to provide quantitative estimates of porosity, pore size and the frequency distribution of pore sizes in the matrices. After pre-processing including conversion to grey scale using Paint Shop Pro (Jasc Software Inc., USA) the rectangular image sections of the samples were processed in order to detect pores using in-house developed software based on MATLAB (The MathWorks Inc., USA). The grey-scale images were filtered, the contrast adjusted and a threshold applied to detect the dark regions of the pores. The same threshold was used for all images in a particular data set, although different thresholds were applied for each sample. Higher level processing involved removing small objects, filtering and removing the image border region prior to calculation of pore areas. Since the image border region was neglected, any pores on the edge of the image (typically six per image slice) were not included in the analysis. For a particular matrix type, the variation of pore area and 'equivalent pore diameter' in each image slice analysed was assessed using MINITAB (Minitab Inc., USA). In addition the pore data for all image slices of a particular sample were used to provide a measure of the frequency distribution of equivalent pore diameters throughout the matrix. The analysis was confined to macropores with equivalent diameter larger than 16.6 µm in view of the resolution of the micro-CT images.

The porosity (%) of PCL matrices after gelatin extraction was estimated using Amira 4.0 (Mercury Computer System Inc., USA) which provides a 3-D data set by visualisation of sequential images. The porosity was calculated by comparing the total pore volume with the total volume of a sample cube (pore phase plus polymeric phase). Each sample of PCL matrix analysed provided 1000 sequential grey-scale images. Blocks of 300 images from top to base of the sample were visualised as 3-D images and the frequency distribution of equivalent pore diameter in each block was determined to assess the uniformity of porosity and hence initial particle distribution through the PCL matrices. The theoretical macroporosity was calculated by dividing the volume of the gelatin particles (pore formers) by the volume of the matrix (gelatin particles plus PCL phase) using a density of $1 gm/cm^3$ for the gelatin particles and the measured density of $0.38 gm/cm^3$ for the microporous PCL phase.

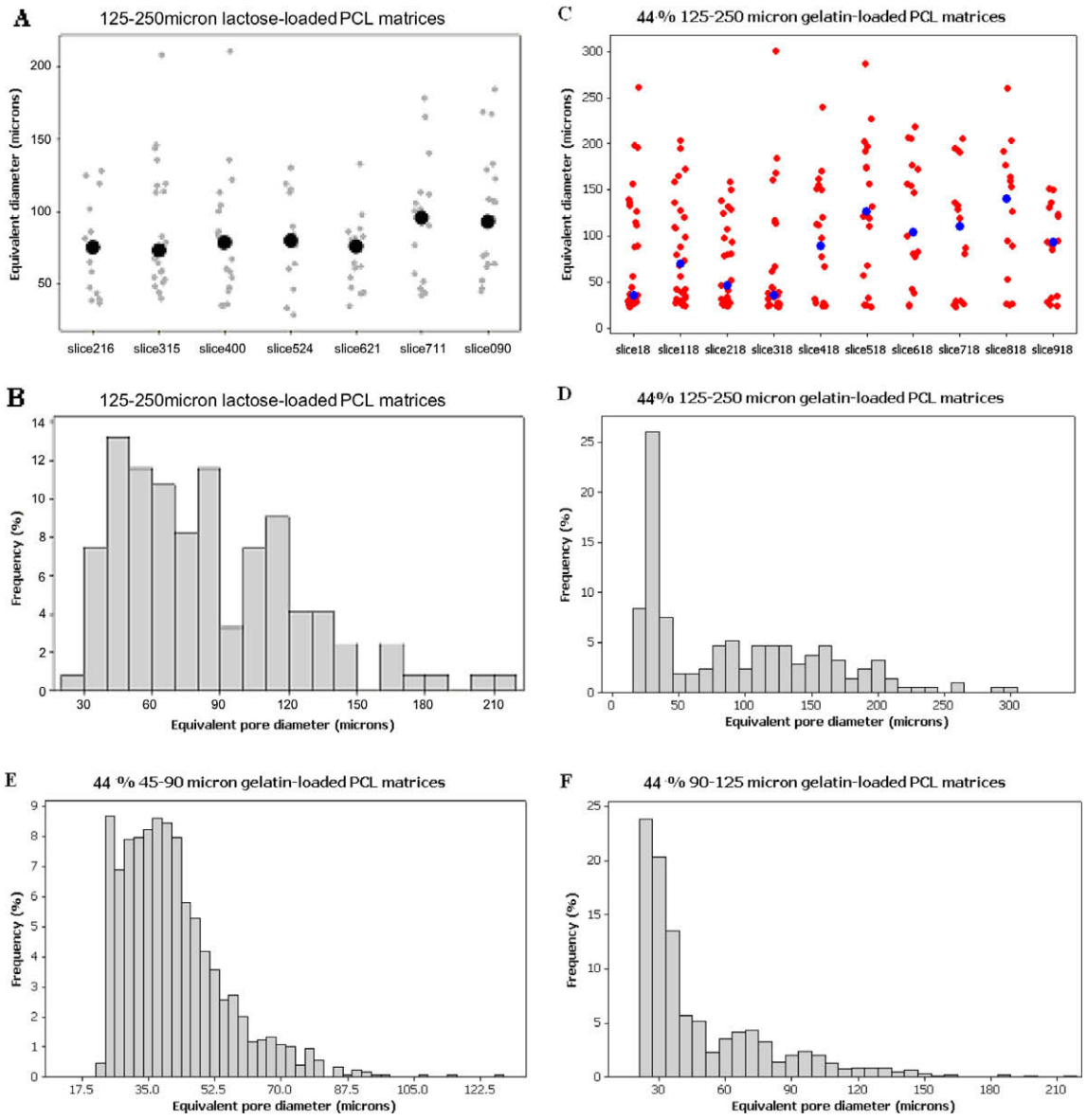

Fig. 6. Analysis of macroporosity using micro-CT images of PCL matrices following extraction of lactose or gelatin particles (A) Variation in equivalent pore diameter (125–250 μm lactose-loaded PCL) (B) Frequency distribution of equivalent pore diameter (125–250 μm lactose-loaded PCL) (C) Variation in equivalent pore diameter (125–250 μm gelatin-loaded PCL) (D) Frequency distribution of equivalent pore diameter (125–250 μm gelatin-loaded PCL) (E) Frequency distribution of equivalent pore diameter (45–90 μm gealtin-loaded PCL) (F) Frequency distribution of equivalent pore diameter (90–125 μm gelatin-loaded PCL).

2.6. Analysis of tortuosity of macroporous PCL matrices

Tortuosity and pore interconnections were investigated by visualisation and analysis using Amira 4.0. A measure of tortuosity was calculated as the ratio of the distance of the path between pores to the straight line distance in 3-D [19].

3. Results and discussion

PCL matrices loaded with 90–125 μm lactose particulates were characterised by a dense surface coating of embedded, 10–20 μm lactose powder 'fines' (Fig. 3A) which gave rise to surface pores of similar size following lactose release (Fig. 3B). Rapid and highly efficient release of lactose occurred from PCL matrices into PBS at 37 °C resulting in over 95% extraction of the initial lactose content in 9 days (Fig. 4). The pronounced burst effect of approximately 75% is conventionally explained by loss of surface located drug molecules and could be conveniently explained by the presence of lactose particles at the matrix surface. However the micro-CT image in Fig. 5B clearly reveals the high concentration of macropores in the matrix interior which are formed by extraction of lactose particulates. Transport of low molecular weight hydrophilic compounds through the PCL matrix is clearly highly efficient but is unlikely to occur through interconnecting macropores formed by particles in contact. The shadow image in Fig. 5C reveals relatively few regions of macropore coalescence. It is considered, therefore, that the main route for lactose transport is provided by the 5–10 μm, microporous structure of the PCL phase which appears to be highly interconnected.

SEM examination of gelatin-loaded PCL matrices revealed deep surface pores in the size range 125–250 μm following particle solubilisation (Fig. 3D) which correspond in size and shape with the original gelatin particle size (Fig. 3F). In addition, surface pores can be seen to connect with underlying pores which assists release

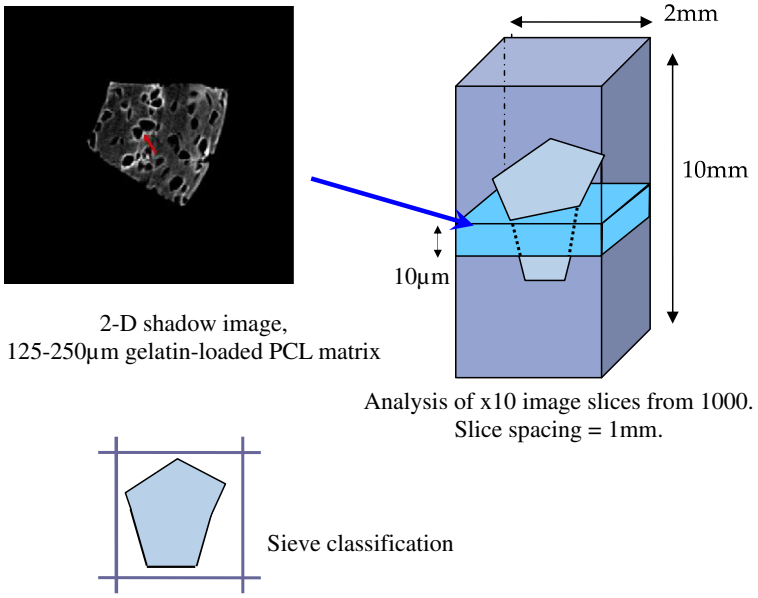

Fig. 7. Schematic illustrating pore size measurement using micro-CT images and particle size classification by sieving.

of protein from the matrix core. Microporosity in the range of 5–10 µm is also visible in the PCL phase (Fig. 3D).

Density differences between the PCL phase (0.38 g/cm^3) and gelatin particulates (1 gm/cm^3) were sufficient to allow resolution of each component of the matrix by micro-CT (Fig. 5D). Subsequent extraction of gelatin enabled definition of the polymer phase (Fig. 5E) and the macropore structure (Fig. 5F). The pore shape and size corresponds closely with the gelatin particles used for matrix production (Fig. 3F) The high pore density following extraction of 29% w/w gelatin-loaded matrices (particle size range 45–90 µm) is particularly striking (Fig. 5G) and tends to suggest that a network of interconnected macropores would be produced due to initial particle contact and subsequent particle dissolution. Close inspection of the 2-D shadow image in Fig. 5H reveals regions of macropore coalescence which provides evidence for the formation of such high volume channels. The connected macropore structure is anticipated to present a 'rapid transit' route for protein molecules, while the 5–10 µm micropores of the PCL phase helps ensure connectivity to achieve the observed high delivery efficiencies in excess of 80%.

Analysis of sequential micro-CT image slices at 1000 µm intervals along the sample long axis enabled detailed information to be gathered on the range of pore sizes and pore size distribution within the matrix (Fig. 6). This data is anticipated to be useful for monitoring sample uniformity and for exploring the relationships between pore architecture, matrix formulation conditions and drug delivery behaviour. The presentation of 'equivalent pore diameters' for 29% w/w lactose (125–250 µm)-loaded PCL matrices in Fig. 6A, reveals low numbers of macropores resulting in a very low fractional pore area of 2.9%. Micro-CT analysis of lactose-loaded PCL matrices is complicated by the presence of 10–20 µm powder 'fines' in the sieved powders which reduces the fraction of large 'primary' particles in the matrix and subsequently the macroporosity. The mean 'equivalent pore diameter' of PCL matrices following solubilisation and release of 125–250 µm lactose particles was around 100 µm which is much smaller than the mean particle size based on sieve classification (188 µm).

The presentation of 'equivalent pore diameters' in sequential image slices for 44% w/w gelatin (125–250 µm)-loaded PCL matrices in Fig. 6C confirms the visual impression of uniformity of pore distribution which is gained from 3-D microtomographs (Fig. 5). A fairly constant mean 'equivalent pore diameter' of 100 µm was obtained. The frequency distribution of pore size (%) (Fig. 6D) indicates that most pores are small around 20–40 µm and some pores are above the size range of sieved particles. This observation may be explained by pore coalescence.

Micro-CT image analysis effectively detected the upper bound of the particle size range used in matrix formulation but recorded a significantly lower pore size than the sieved powder classification (Fig. 6A and C). This tendency may be explained by the 'sectioning effect' of the micro-CT technique used and subsequent analysis of image slices which would not be expected to coincide consistently with the largest dimension of asymmetric pores (Fig. 7). Sieving is designed, in principle, to separate particles based on the largest dimension.

Protein release from PCL matrices containing 44% w/w gelatin particulates was characterised by a major burst effect (80%) during the first 24 h and virtually total protein release in 9 days (Fig. 4). Formation of a highly interconnected pore network within the matrix is indicated, as described above, which facilitates uptake of release medium and protein transport. The rate of protein release was found to be independent of particle size but would be expected to be higher from matrices incorporating small particles since the dissolution rate increases with particle size reduction. This behaviour may be explained by the frequency distribution of pore diameters (Fig. 6D–F) which features a large population of sub-40 µm pores in all gelatin-loaded matrices. Matrix disruption is indicated resulting in a high density of interconnections (pores, fissures) between protein particles which permits rapid protein release.

Micro-CT values of the macroporosity of PCL matrices prepared by extraction of 44% w/w gelatin particles are close to the theoretical value for particle size ranges of 90–125 and 125–250 µm (Table 1). The micro-CT determined macroporosity for PCL matrices produced by extraction of 45–90 µm particles was found to be significantly lower (approximately 50%) than the theoretical value This finding may be explained by the image processing approach, whereby small pores were removed because of noise and image resolution considerations. The data shown here suggest that micro-CT is capable of providing reasonable estimates of macroporosity (within 15% of the theoretical value) for materials containing irregular shaped pores larger than 90 µm. Table 1 also reveals that

Table 1
Macroporosity of PCL matrices determined by analysis of micro-CT images.

Gelatin loading of PCL matrix % w/w	Theoretical macroporosity %	Sample slice number	Macroporosity (%) of PCL matrices prepared by extraction of gelatin particles of three size ranges		
			45–90 μm	90–125 μm	125–250 μm
44	23	001–330	12.3	24.1	26.2
		331–660	12.5	22.7	24.4
		661–1000	11.9	22.9	25.9
		001–1000	12.2	23.1	25.8

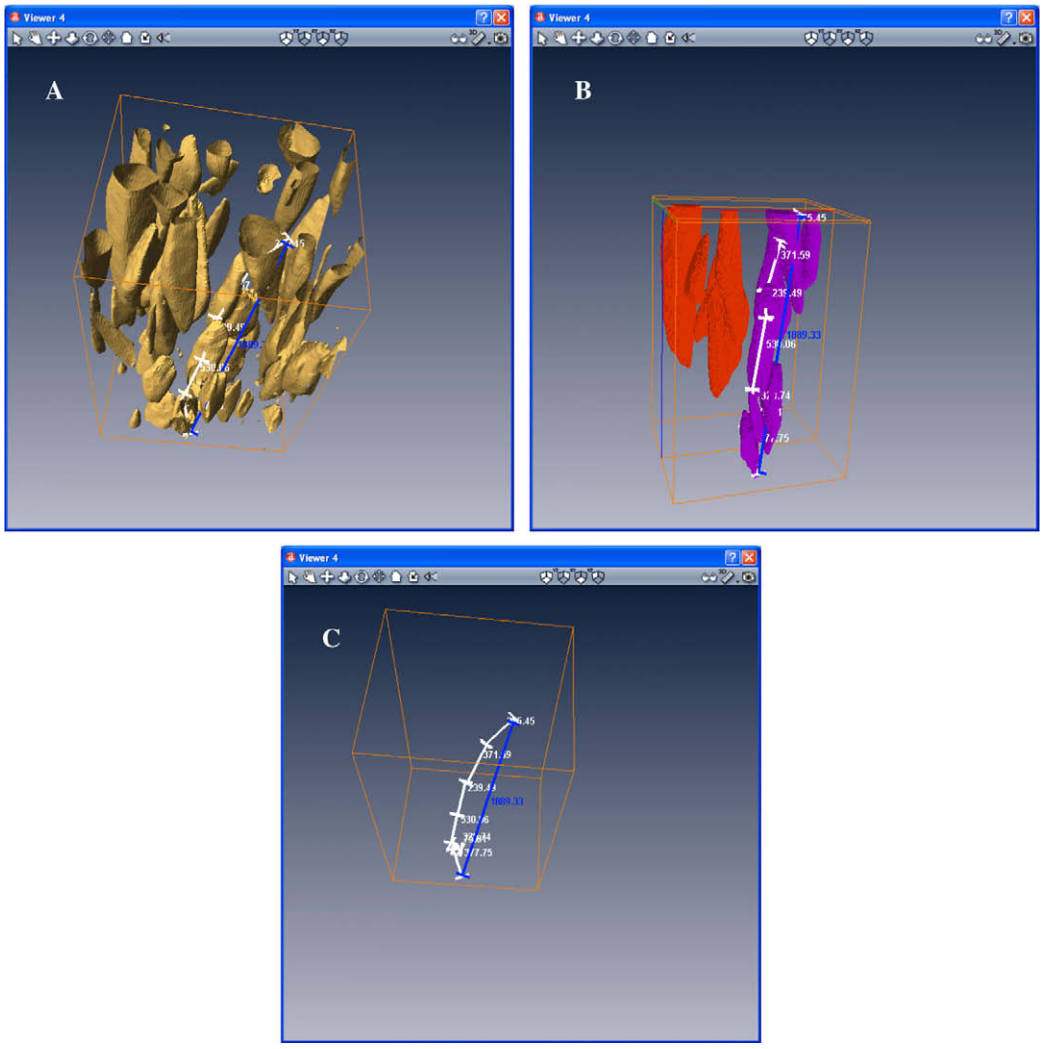

Fig. 8. Step-by-step process of tortuosity analysis (A) isosurface visualisation of pore structure (B) two sets of interconnecting pores (C) path lines for clarity

there is no significant difference in macroporosity from top to base of the sample, demonstrating that high loadings of evenly distributed protein particles may be achieved in PCL matrices using the rapid cooling method.

Tortuosity analysis (Fig. 8) shows an example of two sets of interconnecting pores in red[1] and purple. For the purple set the tortuosity has been calculated as the ratio of the path between pores (shown in white) to the minimum path (shown in blue) and in this example is 1.16.

The upper left image (A) shows an isosurface visualisation of part of a sample from a micro-CT dataset; the isosurface visualisation creates a surface around the pores and hence allows for visualisation through the pores. The upper right image (B) shows two sets of interconnecting pores one in red and the other in purple. For the purple set a value for the tortuosity between the upper and lower points is calculated by drawing lines along a path through the pores (white) and comparing with the straight line distance along the blue line. The lower image (C) shows the path lines only for clarity.

4. Conclusions

Micro-CT offers an advanced analytical technique for characterizing the internal 3-D structure of matrix-type drug delivery devices incorporating particulate bioactives and pore-forming

[1] For interpretation of color in Figs. 1, 4-8, the reader is referred to the web version of this article.

excipients. Analysis of micro-CT images can provide detailed quantitative information on macroporosity for correlation with formulation conditions and drug release behaviour which should lead to improvements in the delivery of small molecule and macromolecular therapeutics.

References

[1] H.I. Chang, Y. Perrie, A.G. Coombes, Delivery of the antibiotic gentamicin sulphate from precipitation cast matrices of polycaprolactone, J. Control. Release 110 (2) (2006) 414–421.
[2] P.D. Darney, Hormonal implants: contraception for a new century, Am. J. Obstet. Gynecol. 171 (1994) 1677.
[3] S. Lin, P.Y. Chao, Y.W. Chien, A. Sayani, S. Kuma, M. Mason, T. Wes, A. Yang, D. Monkhouse, In vitro and in vivo evaluations of biodegradable implants for hormone replacement therapy. Effect of system design and PK–PD relationship, AAPS PharmSciTech 2 (2001) (Article 16).
[4] P. Simamora, S.R. Nadkarni, Y.-C. Lee, S.H. Yalkowski, Controlled delivery of pilocarpine. 2. In-vivo evaluation of gelfoam device, Int. J. Pharm. 170 (1998) 209–214.
[5] E.P. Sipos, B. Tyler, S. Piantadosi, P.C. Burger, H. Brem, Optimizing interstitial delivery of BCNU from controlled release polymers for the treatment of brain tumours, Cancer Chemother. Pharmacol. 39 (1997) 383–389.
[6] M.J. Whitaker, R.A. Quirk, S.M. Howdle, K.M. Shakesheff, Growth factor release from tissue engineering scaffolds, J. Pharm. Pharmacol. 53 (11) (2001) 1427–1437.
[7] P. Costa, J.M. Sousa Lobo, Modeling and comparison of dissolution profiles, Eur. J. Pharm. Sci. 13 (2) (2001) 123–133.
[8] P. Tomlins, P. Grant, S. Mikhalovsky, L. Mikhalovaska, S. James, P. Vadgama, Characterisation of polymeric tissue scaffolds, National Physical Laboratory, UK, Report 89, 2005.
[9] T.P. Foster, E.L. Parrott, Release of highly water-soluble medicinal compounds from inert, heterogeneous matrixes, J. Pharm. Sci. 79 (1990) 806–810.
[10] S.J. Desai, P. Singh, A.P. Simonelli, W.I. Higuchi, Investigation of factors influencing release of solid drug dispersed in inert matrices II, J. Pharm. Sci. 55 (1966) 1224–1229.
[11] K.G. Papadokostaki, S.G. Amarantos, J.H. Petropoulos, Kinetics of release of particulate solutes incorporated in cellulosic polymer matrices as a function of solute solubility and polymer swellability, J. Appl. Polym. Sci. 67 (1998) 227–287.
[12] Y.S. Wu, J. Lucas, H.W. Frijlink, K. Maarscalk, The determination of relative path length as a measure for tortuosity in compacts using image analysis, Eur. J. Pharm. Sci. 28 (2006) 433–440.
[13] J.R. Jones, G. Poologasundarampillai, R.C. Atwood, D. Bernard, P.D. Lee, Non-destructive quantitative 3D analysis for the optimisation of tissue scaffolds, Biomaterials 28 (2007) 1404–1413.
[14] Y. Wang, H.I. Chang, D. Wertheim, A.C. Jones, C. Jackson, A. Coombes, Characterisation of the macroporosity of polycaprolactone-based biocomposites and release kinetics for drug delivery, Biomaterials 28 (2007) 4619–4627.
[15] L.A. Feldkamp, S.A. Goldstein, A.M. Parfitt, G. Jesion, M. Kleerekope, The direct examination of three-dimensional bone architecture in vitro by computed tomography, J. Bone Miner. Res. 4 (1989) 3–11.
[16] J.M. Williams, A. Adewunmi, R. Schek, C.L. Flanagan, P.H. Krebsbach, S.E. Feiberg, S.J. Hollister, S. Das, Bone tissue engineering using polycaprolactone scaffolds fabricated via selective laser sintering, Biomaterials 26 (2005) 4817–4827.
[17] B. Otsuki, M. Takemoto, S. Fujibayashi, M. Neo, T. Kokubo, T. Nakamura, Pore throat size and connectivity determine bone and tissue ingrowth into porous implants: three-dimensional micro-CT based structural analyses of porous bioactive titanium implants, Biomaterials 27 (2006) 5892–5900.
[18] <http://www.digitalscanservice.com/tomography>.
[19] E. Bullitt, G. Gerig, S.M. Pizer, W. Lin, S.R. Aylward, Measuring tortuosity of the intracerebral vasculature from MRA images, IEEE Trans. Med. Imaging 22 (2003) 1163–1171.